Applied Clay Science 47 (2010) 263–270

Contents lists available at ScienceDirect

Applied Clay Science

journal homepage: www.elsevier.com/locate/clay

Effect of modified montmorillonite on biodegradable PHB nanocomposites

Adrian Botana, Mariana Mollo, Patricia Eisenberg, Rosa M. Torres Sanchez *

INTI Plásticos, Gral. Paz 5445, (1650) San Martín, Argentina

ARTICLE INFO

Article history:
Received 27 April 2009
Received in revised form 29 October 2009
Accepted 4 November 2009
Available online 29 November 2009

Keywords:
PHB
Nanocomposites reinforcement
Organo-montmorillonite

ABSTRACT

Polymer nanocomposites, based on a bacterial biodegradable thermoplastic polyester, poly(hydroxybutyrate) (PHB), and two commercial montmorillonites (MT), Na-M (MT) and 30B-M (organically modified MT), were prepared by melt-mixing technique at 165 °C. Both clays minerals were characterized by morphology, crystallochemical parameters, and thermal stability. Lower specific surface area (determined by adsorption methods) values were found for 30B-M. The apparent particle size from light scattering measurements, scanning electron microscopy observations, and crystallite size (determined from XRD patterns) of 30B-M indicated a higher degree of particles exfoliation than of Na-M.

The nanocomposites PHBNa and PHB30B were characterized by differential scanning calorimetry (DSC), polarized optical microscopy (POM), X-ray diffraction (XRD), transmission electron microscopy (TEM), mechanical properties, and burning behaviour. Intercalation/exfoliation observed by TEM and XRD was more pronounced for PHB30B than PHBNa, indicating the better compatibility of 30B-M with the PHB matrix. An increase in crystallization temperature and a decrease in spherullites size were observed for PHB30B. The intercalation/exfoliation observed by TEM and structure XRD increased the moduli of the nanocomposites. The burning behaviour of PHB30B was influenced by the aggregation of the clay mineral particles.

1. Introduction

Montmorillonite, hectorite and saponite are the most commonly used clay minerals for the preparation of polymer nanocomposites. Numerous studies have shown that the incorporation of small quantities of these clay minerals (5–10% in mass), with a certain degree of exfoliated structure, have a great influence on the properties of the final material, such as mechanical strength, stiffness, thermal stability, conductivity, and gas barrier properties (Ray and Okamoto, 2003; Ray and Bousmina, 2005; Tjong, 2006; Ruiz-Hitzky and Van Meerbeek, 2006; Xiong et al., 2007). The nanocomposite structure depends on the clay mineral–polymer compatibility and on processing conditions (Zenggang et al., 2002; Fornes et al., 2003; Homminga et al., 2005; Avella et al., 2006; Cervantes-Uc et al., 2007; Hablot et al., 2008). Mainly, two different structures are achievable: nanocomposites with intercalated or exfoliated clay mineral particles (Ray and Bousmina, 2005; Lagaly et al., 2006). Both structures coexist in nanocomposites, and it is believed that the properties are related to the high aspect ratio of exfoliated structure (Alexandre and Dubois, 2000). The term intercalation (Dennis et al., 2001; Lagaly et al., 2006) describes the case where a small amount of polymer moves into the interlayer space of the clay mineral particles. Exfoliation or delamination occurs when polymer further separates the clay mineral layers, e.g. by 80–100 Å or more.

The use of conventional plastics in the last years has been broadened to new areas. Due to their very low degradation rates, plastics can cause environmental problems when they are disposed as solid waste. An alternative to reduce this problem is the substitution of conventional plastics by biodegradable ones. Polyhydroxybutyrate (PHB) is an example of a biodegradable polymer, obtained from a renewable resource, showing a biodegradation rate of about 3 months after soil burial (Correa et al., 2008). The main applications of PHB are in biomedical, agricultural, and packaging products (Scott, 2002), being the last industry one of the most interested in the use of PHB in form of nanocomposites.

The aim of this study is to characterize two commercial clays minerals (one of them being organically modified) used to prepare PHB nanocomposites.

2. Experimental section

2.1. Materials and methods

2.1.1. Montmorillonite characterization

Na-montmorillonite was Cloisite® Na^+, named Na-M, and organo-montmorillonite was Cloisite® 30B referred to as 30B-M, from Southern Clay Products. Both samples were used as received.

Fig. 1 shows the chemical structure of the quaternary ammonium ion in 30B-M, where T indicates tallow. The amount of the quaternary

* Corresponding author. CETMIC-CCT La Plata, Camino Centenario y 506, (1897) M. B. Gonnet, La Plata, Argentina. Fax: +54 221 4710075.
E-mail addresses: rosats@cetmic.unlp.edu.ar, rosa.torres@gmail.com (R.M. Torres Sanchez).

0169-1317/$ – see front matter © 2009 Elsevier B.V. All rights reserved.
doi:10.1016/j.clay.2009.11.001

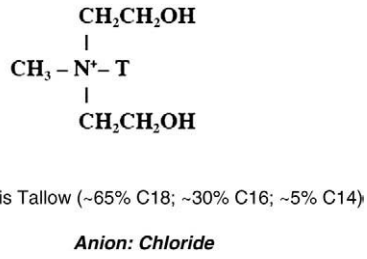

Fig. 1. Quaternary alkylammonium ions exchanged in 30B-M.

ammonium ion corresponded to CEC 0.90 mEq/g as indicated by the supplier.

Chemical analysis (ICP-AES) was performed with Na-M and 30B-M. To decompose the organic material in 30B-M, the sample was heated at 550 °C during 3 h.

The total specific surface area was determined by water vapor adsorption (S_w) at relative humidity 0.56 (Torres Sánchez and Falasca, 1997) while the external specific surface area was determined by nitrogen adsorption (S_{N2}) (BET method, at 77 K) using a Quanta Chrome Autosorb instrument, the interlayer surface (S_I) was obtained as the difference: $S_I = S_w - S_{N2}$. Due to the hydrophobic property of 30B-M, ethyleneglycol (EG), was used to determine the total specific surface area (S_{EG}) (Carter et al., 1965). Pores sizes were determined from adsorption average pore width by BET and BJH methods.

Particle size determination was performed by dynamic light scattering DLS measurements with a Brookhaven 90Plus/Bi-MAS Multi Angle Particle Sizing, operating at $\lambda = 635$ nm, 15 mW solid state laser, scattering angle 90°, 25 ± 0.1 °C. The samples were dispersed in EtOH/water (1:1) with solid contents of 1% by mass. The apparent equivalent sphere diameter (D_{app}) was determined.

Morphology was determined by Scanning Electron Microscopy (Philips 515).

A Philips 3020 apparatus was used to record X-ray diffraction (XRD) patterns. The operating conditions were: 40 kV and 30 mA, Cu K_α radiation, Ni filter. Diffraction data were collected over a 2θ range of 3°–70°, with a step width of 0.02° and a counting time of 2.0 s/step. Semi-oriented air- dried samples, maintained at relative humidity of 0.47 for 12 h were analyzed by means of the powder mounting technique. Crystallographic parameters were evaluated from the 001 reflection. The crystallite sizes were calculated using the Scherrer formula taking into account the instrumental broadening (Cullity, 1978).

Temperature of dehydration was achieved by differential thermal analysis (DTA) on a STA 409/c Netzsch, on 200 mg samples, (temperature ramp 10 °C/min, calcined alumina as reference inert material, air atmosphere).

2.1.2. Nanocomposites

The PHB homopolymer "Biocycle 1000" (PHB Industrial S.A., Brazil) and Na-M or 30B-M were dried under vacuum at 60 °C during 24 h before use. The nanocomposites were prepared by melt intercalation in an internal mixing chamber Brabender Plasticorder (30 cm^3) at 165 °C and a rotor speed of 50 rpm for 10 and 30 min. Na-M and 30B-M content were fixed at 5% m/m, and the composites obtained were denoted as PHBNa and PHB30B. The same mixing procedure was used for pure PHB for comparison.

The thermal behaviour was investigated by differential scanning calorimetry (DSC Mettler 822e/500/1473) at a heating rate of 10 °C/min and cooling rate of 5 °C/min, under nitrogen atmosphere. Non-isothermal crystallization from the melt was carried out by heating the sample to 220 °C and maintaining it at that temperature for 10 min to eliminate residual crystals, cooling at 5 °C/min to 50 °C. The sample was then heated to 200 °C at 10 °C/min to record the melting process.

Crystal morphology was investigated by polarized optical microscopy (POM) (Leitz Wetzlar). The samples were melted between two glass plates and maintained at 100 °C for 40 min to control the crystallization process.

The dispersion of the montmorillonite particles and the degree of intercalation/exfoliation in the nanocomposites were determined by XRD analysis and transmission electron microscopy (TEM).

The XRD patterns of nanocomposite films were prepared by thermo-compression molding.

TEM analysis was done with a Jeol 100-CX, at 100 kV. Samples were cut (approximately 50 nm thick) with a cryo-ultra microtome (LEICA UST) operated at −90 °C.

Tensile testing was performed at 23 °C at a constant rate of 1 mm/min, with an INSTRON universal tensile tester model 1125, and ribbon-shape specimens (10 mm width).

The burning behaviour of the nanocomposites was visually observed following an adapted procedure from the Vertical Burning Test (UL94), where a set of specimens were exposed to a standard test flame.

3. Results and discussion

3.1. Clay minerals

Similar elemental contents were found in both samples (Table 1). The decrease of the Na_2O and CaO of the heated 30B-M was indicative of the amount of quaternary ammonium ions bound. LOI was low due

Table 1
Chemical analysis of indicated samples.

Sample	SiO_2	Al_2O_3	Fe_2O_3	Na_2O	CaO	MgO	K_2O	TiO_2	BaO	MnO	Cr_2O_3	P_2O_5	LOI*
	%	%	%	%	%	%	%	%	%	%	%	%	%
Na-M	56.70	19.15	4.18	3.55	0.13	2.11	0.05	0.11	<0.01	0.01	<0.01	0.02	12.05
30B-$M_{calcined}$	62.10	21.10	4.57	0.38	0.06	2.24	0.06	0.13	<0.01	0.01	<0.01	0.05	7.40

* LOI: loss on ignition.

Table 2
Specific surface area (S_{N2}, S_w and S_I), pore size and average pore width and apparent particles size D_{app}.

Sample	S_{N2} (m^2/g)	*C* value	BET pore size (μm)	BJH pore width (μm)	S_w (m^2/g)	S_I ($S_w - S_{N2}$)	S_{EG}	Apparent particles size D_{app} (μm)
Na-M	19.3	102	1.2	1.5	483	464	550	2.6
30B-M	10.0	21	1.7	2.7	91	81	95	4.8

to the reduced amount of interlamellar water and the preceding calcination.

The structural formulae were determined following Siguin et al. (1994) from chemical composition (Table 1):

$$Na - M(Si_{3.97}Al_{0.03})[Al_{1.56}Fe_{0.22}Mg_{0.22}]_{0.25}M^{+}$$

$$\text{calcined } 30B - M(Si_{3.97}Al_{0.03})[Al_{1.57}Fe_{0.22}Mg_{0.21}]_{0.24}M^{+}$$

The coincidence of both structural formulae allows us to assume that the same raw material was used in the industrial preparation of Na-M and 30B-M.

The specific surface area value of Na-M was similar to values determined for other natural montmorillonite samples (Altin et al., 1999; Lombardi et al., 2003; Kádár et al., 2006). Ion exchange with the alkylammonium ions reduced the specific surface area (Kádár et al., 2006). The increase of the average pore width 30% (30B-M) and 56% (Na-M) corresponded to the surface area values.

Also, the *C* value of the BET equation was lower for 30B-M and indicated a stronger interaction between Na-M and nitrogen (Kádár et al., 2006).

The specific surface area values, obtained by water (S_w) and EG (S_{EG}) adsorption on Na-M were in agreement with those determined for montmorillonites of similar chemical composition (Lombardi et al., 2002; Magnoli et al., 2008). S_w and S_{EG} were closer to the values of completely exfoliated montmorillonite particles (Santamarina et al., 2002) than the BET specific surface area. Organic modification of the montmorillonite also reduced S_w and S_{EG} (Table 2).

The higher apparent particle size, D_{app}, of the 30B-M particles may be related to the enhanced aggregation of the particles.

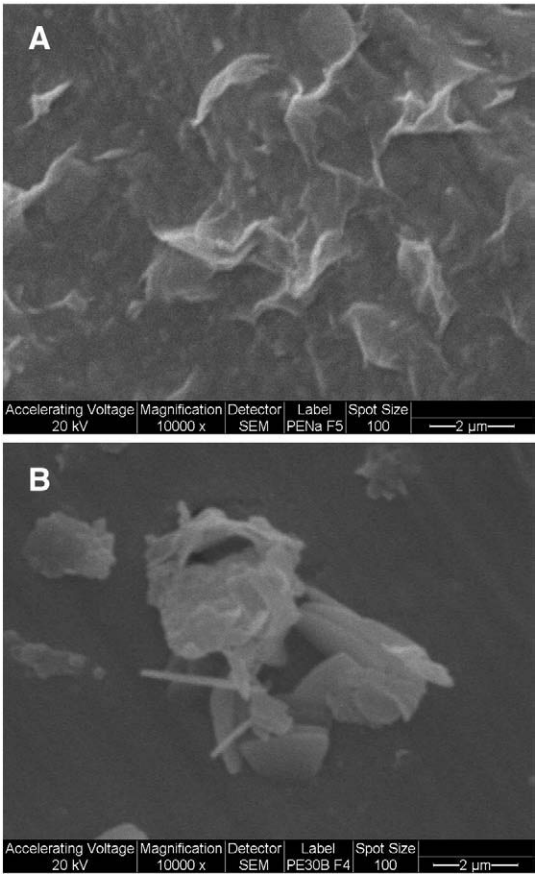

Fig. 2. Scanning electron microscopy (SEM) of (A) Na-M and (B) 30B-M (bar indicates 2 μm).

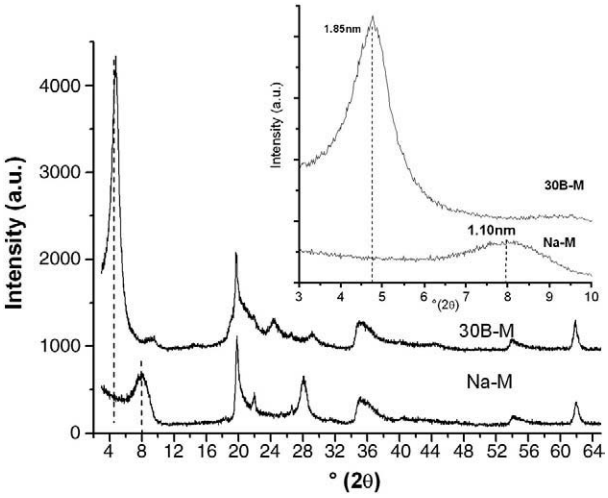

Fig. 3. XRD patterns. The curves are vertically offset for clarity.

3.2. Morphology

Na-M and 30B-M indicated a similar average particle size of 2 μm (Fig. 2). The massive and curved sheets of Na-M (Lee and Kim, 2002) changed into aggregated particles of 30B-M and the sheets became relatively flat as also found by He et al. (2006). SEM microphotographs also revealed pronounced edge–edge contacts between Na-M particles which may indicate a higher degree of particle exfoliation, in agreement with the D_{app} values (Table 2).

3.3. X-ray diffraction

The basal spacing $d(001) = 1.10$ nm for Na-M shifted to 1.85 nm for 30B-M (Fig. 3). Using the HyperChem release 7.5 software, the size parameters of the quaternary ammonium ion were determined as 0.53 nm height, 0.60 nm thickness and 2.59 nm length.

Crystallochemical parameters derived from the (001) reflection are reported in Table 3, which shows the variation of the position (2θCuKα), basal spacing $d(001)$, full width half maximum ($\Delta°2\theta$) value (FWHM) and crystallite size of the samples.

3.4. Differential thermal analysis

As nanocomposites materials were prepared by melt processing followed by thermo-compression molding (165 °C and 180 °C, respectively), thermal decomposition of 30B-M needs to be evaluated (Fig. 4).

Na-M showed the classical water release: at 130 °C a mass loss of 8% due to free water and at 674 °C corresponding to a structural water loss of 4.9% (Ton-That et al., 2004; Cervantes-Uc et al., 2007; Belardi et al., 2007; Vazquez et al., 2008). The exothermic peak at 929 °C is due to recrystallization (Acemana et al., 1999). 30B-M (which has two hydroxyl groups in the alkylammonium ion) showed the free water loss of 2% at 80 °C. The higher amount of free water released from Na-M with respect to 30B-M is related to the presence of OH groups in the

Table 3
Crystallographic parameters derived from the (001) basal reflection (semi-oriented samples) of XRD patterns for indicated samples.

(001) reflection	Position (2θ CuKα)	*d* (001) (nm)	FWHM ($\Delta°2\theta$)	Crystallite size (nm)
Na-M	7.78	1.10	1.79	2.28
30B-M	4.78	1.85	0.98	7.75

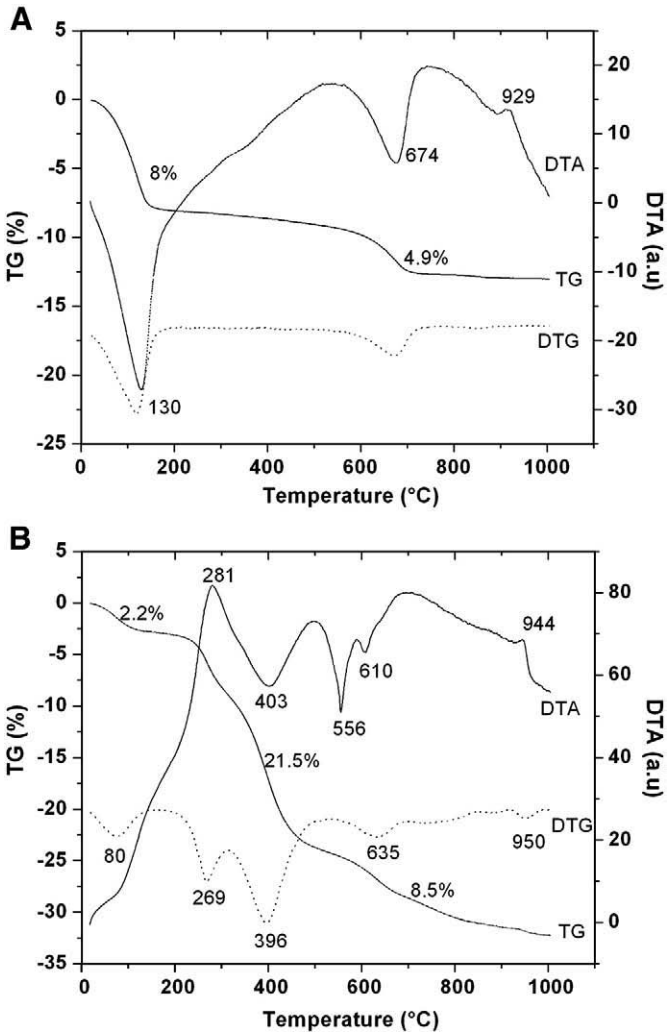

Fig. 4. DTA analysis: (A) Na-M and (B) 30B-M.

alkylammonium ions substitution in the montmorillonite interlayer space. The mass loss in the temperature range from 200 to 600 °C (21.5%) was assigned not only to structural water but also to decomposition of the alkylammonium ions at 297 °C–427 °C (Cervantes-Uc et al., 2007). The peak at 610 °C was also attributed to some structural water release, equivalent to the 674 °C peak for Na-M. For 30B-M the peak appeared at lower temperature due to the lower silicate amount of 30B-M. The exothermic peak at 281 °C was associated to the CO_2 desorption (Cervantes-Uc et al., 2007) while that at 944 °C was related to the recrystallization of montmorillonite. The shift to a higher temperature with respect to Na-M may be related to a different amorphous structure formed after the decomposition of the alkylammonium ions.

Thermal stability of Na-M indicates that only free water will be affect during the processing conditions of the nanocomposites.

For Cloisite 30B the onset decomposition temperature obtained by Cervantes-Uc et al. (2007) was 174 °C compared to around 200 °C in our study, probably caused by the nanocomposite processing conditions (time and shear stress).

3.5. Nanocomposite compounding

The potential property improvements due to incorporation of clay mineral particles into a polymeric matrix usually depends on the dispersion and the degree of delamination, which results from the proper clay chemical modification and polymer–particle interactions and optimized processing conditions.

It is well documented that organic modification influences the degree of dispersion of the montmorillonite particles in the matrix. Dennis et al. (2001) studied the effect of shear stress on the degree of delamination and dispersion of the montmorillonite particles in the polymer matrix. Very high shear was not the key to delamination for the system polypropylene/Cloisite 30B. They explained that polymer chains must enter the interlayer spaces to enhance delamination. This process in promoted by higher residence times during the process and lower polymer matrix molecular mass. Thus the mixing time may be of influence.

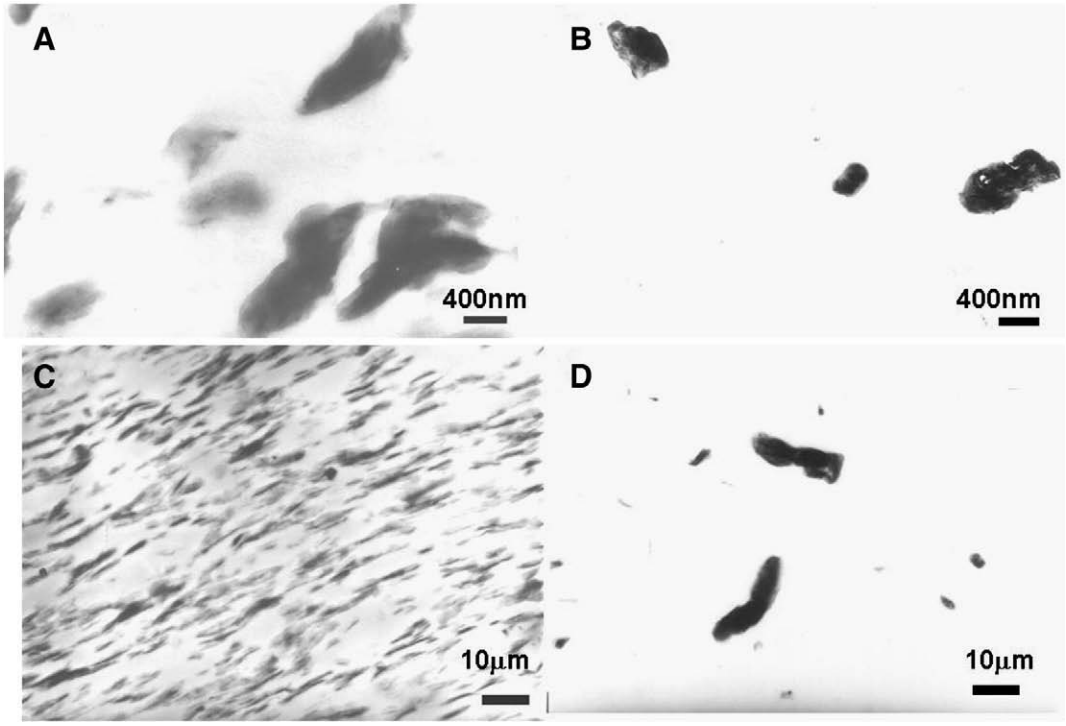

Fig. 5. TEM micrographs (A) PHB/30B-M, 10 min; (B) PHB/Na-M, 10 min; (C) PHB/30B-M, 30 min; (D) PHB/Na-M, 30 min.

Table 4
Mechanical properties for indicated samples.

Sample	Modulus [GPa]	Tensile strength [MPa]
PHB Biocycle 1000 (PHB Industrial)	2.5–3.0	30–40
PHB	3.06	29.6
PHBNa	3.20	24.9
PHB30B	3.44	27.0

PHB and PHB with 5% of Na-M and 30B-M were mixed 10 and 30 min in a Brabender mixing chamber. After 10 min, similar dispersion was observed for both clay minerals. For PHB/30B-M after 10 min, TEM micrographs showed (at higher magnifications) some intercalation, but the dispersion was poor. Increased mixing time improved 30B-M dispersion (Fig. 5). Thus better dispersion of 30B-M was obtained after 30 min of mixing. During 30 min of mixing the thermal degradation has to be considered.

The PHB thermal degradation during processing occurs even at lower temperatures than the melting point. This fact requires a narrow PHB processing window. Thermal degradation of PHB has been suggested to occur by a non-radical random chain scission reaction, with a decrease in the macromolecular length (Aoyagi et al., 2002; Yamaguchi and Arakawa, 2006). As a mixing time of 30 min could cause thermal degradation of PHB, mechanical properties of PHB and PHB nanocomposites were measured in order to evaluate the influence of processing conditions (mixing time) (Table 4).

No difference was observed of the tensile strength and modulus for PHB mixed during 30 min compared to the technical datasheet (PHB Industrial S.A.). In a semicrystalline polymer, as PHB, the relative amount of amorphous and crystalline phases strongly influences the mechanical properties (Rosen, 1993). To study the effect of molecular mass decrease, due to thermal degradation, on crystallinity and then on mechanical properties, PHB unprocessed and processed 30 min was investigated by differential scanning calorimetry.

DSC showed no difference in the degree of crystallization (68%), melting point and endothermic peak shape (Fig. 6). The decrease in molecular mass due to thermal degradation during mixing (Aoyagi et al., 2002; Yamaguchi and Arakawa, 2006) showed no significant influence on the PHB crystalline structure. Similar crystalline structures lead to the similar mechanical properties of processed and unprocessed PHB (Table 4).

The presence of the alkylammonium ions in 30B-M could also affect the thermal stability of PHB. Bordes et al. (2009) studied the influence of the modifier on PHB degradation. A decrease in thermal stability was found for 3% surfactant content. In our study the nanocomposite was prepared using 5% 30B-M which involved 1% of organic modifier (0.90 mEq/g 30B-M). Our results showed that this surfactant amount had no significant effect on the mechanical properties of the nanocomposites (Table 4).

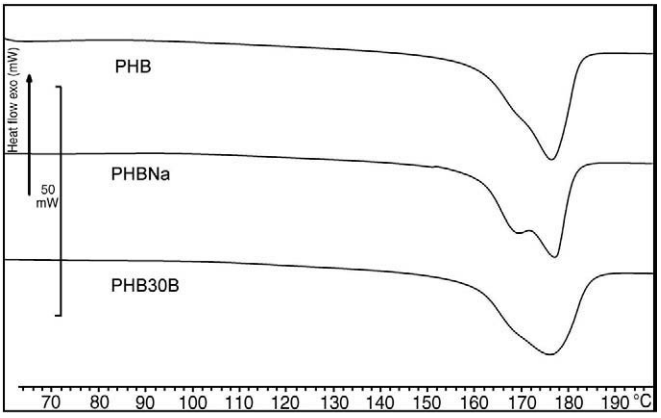

Fig. 7. DSC thermograms. Second heating runs for PHB, PHBNa and PHB30B.

Considering the results describe above, the processing conditions chosen for PHB nanocomposite preparation were 165 °C, rotor speed of 50 rpm and 30 min mixing time.

3.6. Differential scanning calorimetry and polarized optical microscopy

The DSC curves of PHB and PHB nanocomposites (Fig. 7, second heating run) showed, during the first and second heating, a secondary melting temperature at $T_{m2}<T_{m1}$, already observed by Oliveira et al. (2006). Multiple melting behaviours are usually due to melting of crystals with different lamellar thickness. For nanocomposites, both T_{m1} and T_{m2} (second run) were lower than of PHB. This may be related to a slight reduction in crystal size and lower degree of crystallinity as a result of the restricted polymer chain mobility in the presence of the filler (Jiménez et al., 1997; Ogata et al., 1997; Di Maioa et al., 2004). A significant difference in the melting peaks for PHBNa and PHB30B was not observed.

Non-isothermal crystallization curves from the melt (Fig. 8) indicated an increase in the crystallization temperature (T_c) of the nanocomposites relative to PHB. The crystallization time $t_c=(T_i-T_e)/r$ (where $r=5$ °C/min, T_i and T_e are onset and endset temperatures of crystallization peak) (Fig. 9) decreased for PHB, PHBNa and PHB30B.

The polarized optical micrographs (Fig. 10) indicated difference of the spherullite size.

Differences observed in T_c, t_c and spherullites sizes indicated that the clay minerals acted as nucleating agents causing a higher crystallization rate. A similar behaviour was observed by Maiti et al. (2007) and Bordes et al. (2008) for PHB nanocomposites.

When PHB crystallizes in the presence of the clay mineral particles, crystals could grow on the particle surfaces. PHBNa showed larger spherullites than PHB30B. This result may be related to the enhanced

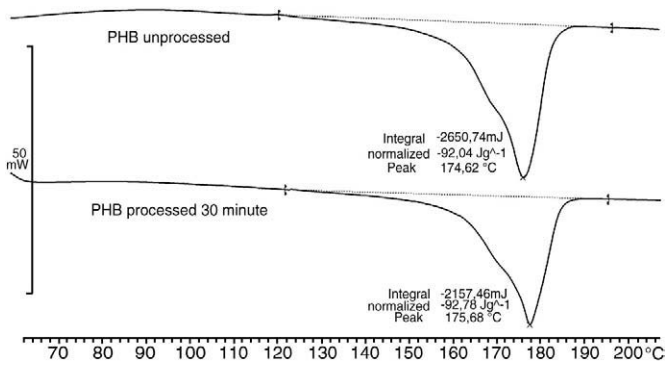

Fig. 6. DSC thermograms: PHB unprocessed and PHB processed 30 min.

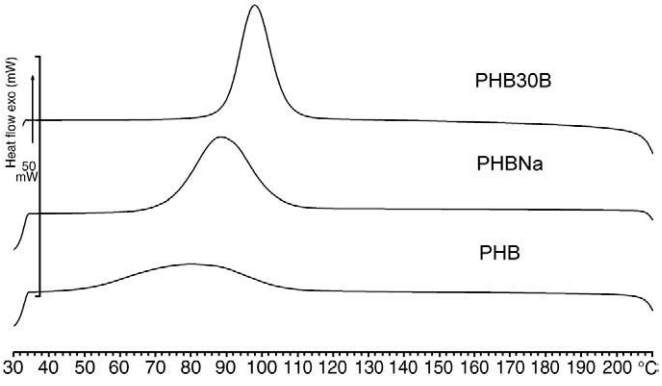

Fig. 8. Non-isothermal crystallization (DSC thermograms).

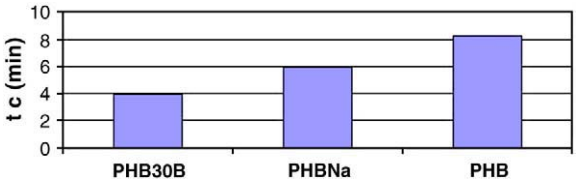

Fig. 9. Crystallization times of PHB and the nanocomposites.

intercalation/exfoliation of 30B-M particles in the PHB matrix as indicated by TEM.

3.7. X-ray diffraction

Main reflections of PHB were still present in both nanocomposites (Fig. 11). The (001) reflection of Na-M and 30-M was slightly shifted to lower angles in the nanocomposites indicating an interlayer

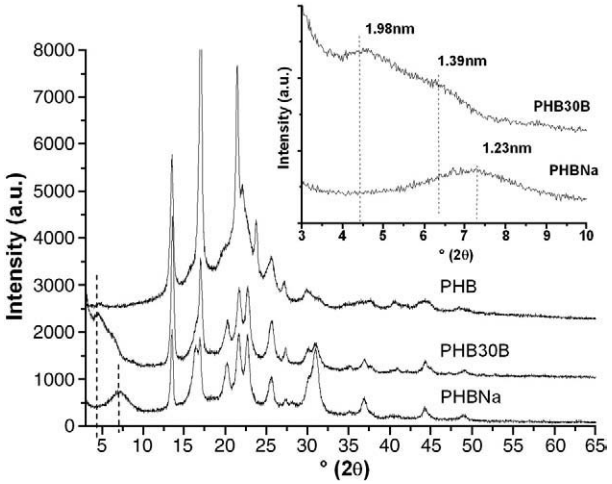

Fig. 11. XRD patterns of PHB, PHBNa and PHB30B.

expansion of 0.13 nm. The shape of the (001) reflection of PHBNa was similar to Na-M (Fig. 3). However, for PHB30B a much larger broadening and decreasing intensity of the (001) reflection was observed. Vaia and Giannelis (1997) explained that this behaviour is due to a decrease in the degree of coherent layer stacking (i.e. a more disordered system).

For PHB30B (right corner Fig. 11), two reflections were observed indicating spacings of 1.98 nm and 1.39 nm. The second spacing was indicative of the collapse of interlayer space due to the thermal degradation of the alkylammonium ions during nanocomposites processing (Ryu et al., 2002).

Lower magnification of TEM images (Fig. 5C and D) indicated better dispersion of 30B-M particles in the PHB matrix whereas Na-M formed aggregates. Higher magnification (Fig. 12) showed intercalated 30B-M particles in agreement with the XRD patterns.

3.8. Mechanical properties

The ANOVA evaluation of the tensile properties data (Table 4) showed that the addition of the clay mineral particles affected the mechanical properties of the nanocomposites. The modulus of PHB30B and PHBNa was increased compared to pure PHB. The higher modulus of PHB30B represented the better particle exfoliation/intercalation. Other authors (Maiti et al., 2007; Bordes et al., 2008) observed a similar increase in the elastic modulus for PHB nanocomposites prepared by melt intercalation. Zhang et al. (2007) reported an increased elastic modulus of poly(hydroxybutyrate-co-3-hydroxyhexanoate) nanocomposites up to 5% of clay mineral addition. They also observed

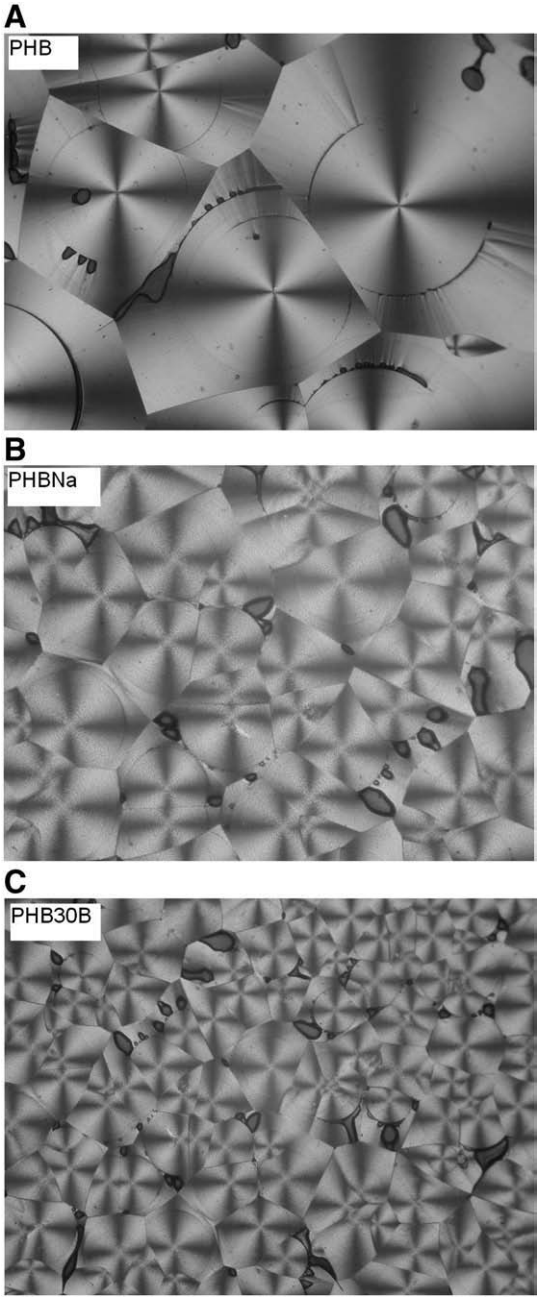

Fig. 10. Polarized optical microscopy photographs of PHB, PHBNa and PHB30B.

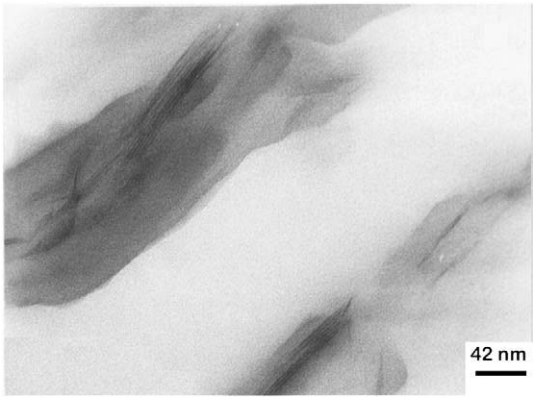

Fig. 12. High magnification TEM micrograph of PHB30B (bar indicates 42 nm).

that larger amounts of the clay mineral did not improve the Young modulus and tensile strength. A similar trend was observed for other systems, such as polylactid acid/montmorillonite (Chang et al., 2003).

The tensile strength of the nanocomposites showed no significant difference to processed PHB. For a similar system, Bordes et al. (2008) reported a 15% increase in tensile strength after addition of organo-modified montmorillonite, and the same behaviour was observed for other systems, such as aliphatic biodegradable polyesters (APES) (Lee et al., 2002). Pavlidou and Papaspyrides (2008) pointed out that the intercalation/exfoliation ratio is the main factor responsible for the improvement of mechanical properties. They proposed that exfoliated particles are responsible for improvement in stiffness, while intercalated play minor role. TEM images of PHB30B showed a high intercalation degree, responsible for the increase in tensile modulus, but according to Pavlidou and Papaspyrides, the exfoliation/intercalation ratio was not high enough to increase the tensile strength compare to PHB matrix.

3.9. Burning characteristics

For PHB and PHBNa a constant liquid burning dripping was observed until the probe was totally consumed by combustion. For PHB30B no liquid dripping was observed. Similar results were found for polyurethane (Berta et al., 2006) and polycaprolactone nanocomposites (Lepoittevin et al., 2002). The burned probe maintained its integrity at the end of the test, probably due to the aggregated 30B-M.

4. Conclusions

The apparent particle diameters from light scattering measurements indicated aggregated particles of 30B-M. The montmorillonite particles acted as a nucleating agent in the PHB matrix. PHB30B TEM images showed better particle dispersion and intercalation than PHBNa, due to a compatibility between the organic modified montmorillonite and PHB which may be responsible for the higher Young modulus obtained. However, the exfoliation/intercalation ratio was not high enough to increase the tensile strength. PHB30B maintained its integrity after burning, probably due to the aggregated 30B-M particles. These preliminary results encourage to optimize these PHB nanocomposites.

Acknowledgements

The authors thank ANPCyT PICT 1360 and NOVELQ: Novel Processing Methods for the Production and Distribution of High-Quality and Safe Foods contract no: 015710- for financial support.

References

Acemana, S., Lahav, N., Yariv, S., 1999. A Thermo-FTIR spectroscopy analysis of Al-pillared smectites differing in source of charge in KBr disks. Thermochim. Acta 340–341, 349–366.
Alexandre, M., Dubois, P., 2000. Polymer-layered silicate nanocomposites: preparation, properties and uses of a new class of materials. Mater. Sci. Eng. 28, 1–63.
Altin, O., Ozberge, O., Dogu, T., 1999. Effect of pH, in an aqueous medium, on the surface area, pore size distribution, density and porosity of montmorillonite. J. Colloid Interface Sci. 217, 19–27.
Aoyagi, Y., Yamashita, K., Doi, Y., 2002. Thermal degradation of Poly([R]-3-hydroxybutyrate], Poly[ε-caprolactone], and poly[(S)-lactide]. Polym. Degrad. Stab. 79, 53–59.
Avella, M., Bondioli, F., Canillo, V., Di Pace, E., Errico, M.E., Ferrari, A.M., Focher, B., Malinconico, M., 2006. Poly(ε-caprolactone)-based nanocomposites: influence of compatibilization on properties of poly(ε-caprolactone)-silica nanocomposites. Compos. Sci. Technol. 66, 886–894.
Belardi, H., Haouzi, A., Couillard, J.M., Giuntini, J.C., Henn, F., 2007. Hydration of Na^+-montmorillonite studied by thermally stimulated depolarization current. J. Colloid Interface Sci. 308, 216–221.
Berta, M., Lindsay, C., Pans, G., Camino, G., 2006. Effect of chemical structure on combustion and thermal behaviour of polyurethane elastomer layered silicate nanocomposites. Polym. Degrad. Stab. 91, 1179–1191.
Bordes, P., Pollet, E., Bourbigot, S., Avèrous, L., 2008. Structure and porperties of PHA/Clay nano-biocomposites prepared by melt intercalation. Macromol. Chem. Phys. 209, 1473–1484.
Bordes, P., Hablot, E., Pollet, E., Avérous, L., 2009. Effect of clay organomodifiers on degradation of polyhydroxyalkanoates. Polym. Degrad. Stab. 94, 789–796.
Carter, D.L., Heilman, M.D., Gonzalez, C.L., 1965. Ethylene glycol monoethyl ether for determining surface area of silicate minerals. Soil Sci. 100 (5), 356–360.
Cervantes-Uc, J.M., Cauich-Rodrıguez, J.V., Vazquez-Torres, H., Garfias-Mesıas, L.F., Pau, D.R., 2007. Thermal degradation of commercially available organoclays studied by TGA-FTIR. Thermochim. Acta 457, 92–102.
Chang, J., An, Y.U., Cho, D., Giannelis, E.P., 2003. Poly(lactid acid) nanocomposites: comparison of their properties with montmorillonite and synthetic mica (II). Polymer 44, 3715–3720.
Correa, M.C.S., Rezende, M.L., Rosa, D.S., Agnelli, J.A.M., Nascente, P.A.P., 2008. Surface composition and morphology of poly(3-hydroxybutyrate) exposed to biodegradation. Polym. Test. 27, 447–452.
Cullity, D., 1978. Elements of X-ray Diffraction. Addison-Wesley Publishing Co., Reading, Massachusetts.
Dennis, H.R., Hunter, D., Chang, D., Kim, S., White, J.L., Cho, J.W., Paul, D.R., 2001. Effect of melt processing conditions on the extent of exfoliation in organoclay-based nanocomposites. Polymer 42, 9513–9522.
Di Maioa, E., Iannace, S., Sorrentino, L., Nicolaisa, L., 2004. Isothermal crystallization in PCL/clay nanocomposites investigated with thermal and rheometric methods. Polymer 45, 8893–8900.
Fornes, T., Yoon, P., Paul, D., 2003. Polymer matrix degradation and color formation in melt processed nylon 6/clay nanocomposites. Polymer 44, 7545–7556.
Hablot, E., Bordes, P., Pollet, E., Avérous, L., 2008. Thermal and thermo-mechanical degradation of poly (3-hydroxybutyrate)-based multiphase systems. Polym. Degrad. Stab. 93, 413–421.
He, H., Frost, R.L., Bostrom, T., Yuan, P., Duong, L., Yang, D., Xi, Y., Kloprogge, J.T., 2006. Changes in the morphology of organoclays with $HDTMA^+$ surfactant loading. Appl. Clay Sci. 31, 262–271.
Homminga, D., Goderis, B., Hoffman, S., Reynaers, H., Groeninckx, G., 2005. Influence of shear flow on the preparation of polymer layered silicate nanocomposites. Polymer 46, 9941–9954.
Jiménez, G., Ogata, N., Kawai, H., Ogihara, T., 1997. Structure and thermal/mechanical properties of poly (-caprolactone)-clay blend. J. Appl. Polym. Sci. 64, 2211–2215.
Kádár, F., Szazdi, L., Fekete, E., Pukanszky, B., 2006. Surface characteristics of layered silicates: influence on the properties of clay/polymer nanocomposites. Langmuir 22, 7848–7854.
Lagaly, G., Ogawa, M., Dekany, I., 2006. Handbook of Clay Sci. Chap. In: Bergaya, F., Theng, B.K., Lagaly, G. (Eds.), Clay Mineral organic interactions. Elsevier, Amsterdam.
Lee, S.Y., Kim, S.J., 2002. Expansion characteristics of organoclay as a precursor to nanocomposites. Colloids Surf., A Physicochem. Eng. Asp. 211, 19–26.
Lee, S., Park, H., Lim, H., Kang, T., Li, X., Cho, W., Ha, C., 2002. Microstructure, tensile properties, and biodegradability of aliphatic polyester/clay nanocomposites. Polymer 43, 2495–2500.
Lepoittevin, B., Devalckenaere, M., Pantoustier, N., Alexandre, M., Kubies, D., Calberg, C., Jérôme, R., Dubois, P., 2002. Poly(ε-caprolactone)/clay nanocomposites prepared by melt intercalation: mechanical, thermal and rheological properties. Polymer 43, 4017–4023.
Lombardi, B., Baschini, M., Torres Sánchez, R.M., 2002. Characterization of montmorillonites from bentonite deposits of North Patagonia, Argentina: physicochemical and structural parameter correlation. J. Arg. Chem. Soc. 90 (4–6), 87–99.
Lombardi, B., Baschini, M., Torres Sánchez, R.M., 2003. Bentonite deposits of Northern Patagonia. Appl. Clay Sci. 22, 309–312.
Magnoli, A., Tallone, L., Dalcero, M.A., Chiacchiera, S.M., Torres Sanchez, R.M., 2008. Structural characteristic of commercial bentonites used as detoxifier of broiler feed contamination with aflatoxin. Appl. Clay Min. 40, 63–71.
Maiti, P., Batt, C.A., Giannelis, E.P., 2007. New biodegradable polyhydroxybutyrate/layered silicate nanocomposites. Biomacromolecules 8, 3393–3400.
Ogata, N., Kawakage, S., Ogihara, 1997. Structure and thermal/mechanical properties of poly(ethylene oxide)-clay mineral blends. Polymer 38 (20), 5115.
Oliveira, L.M., Araújo, E.S., S.M.L., Guedes, S.M., 2006. Gamma irradiation effects on poly (hydroxybutyrate). Polym. Degrad. Stab. 91, 2157.
Pavlidou, S., Papaspyrides, C.D., 2008. A review on polymer-layered silicate nanocomposites. Prog. Polym. Sci. 33, 1119–1198.
Ray, S., Bousmina, M., 2005. Biodegradable polymers and their layered silicate nanocomposites: in greening the 21st century materials world. Prog. Mater. Sci. 50, 962–1079.
Ray, S., Okamoto, M., 2003. Polymer/layered silicate nanocomposite: a review from preparation to processing. Prog. Polym. Sci. 28, 1539–1641.
Rosen, S.L., 1993. Fundamental Principles of Polymeric Materials, 2nd Ed. John Wiley & Sons, Inc.
Ruiz-Hitzky, E., Van Meerbeek, A., 2006. Handbook of Clay Sci. Chap. In: Bergaya, F., Theng, B.K., Lagaly, G. (Eds.), Clay Mineral- and organoclay-4 polymer nanocomposite. Elsevier, Amsterdam.
Ryu, J.G., Lee, J.W., Kim, H., 2002. Development of poly(methyl metacrylate)-clay nanocomposites by using power ultrasonic wave. Macromol. Res. 10 (4), 187–193.
Santamarina, J.C., Klein, K.A., Wang, Y.H., Prencke, E., 2002. Specific surface: determination and relevance. Can. Geotech. J. 39, 233–241.
Scott, A., 2002. Biodegradable polymers from food waste. Chemical Week 164 (48), 24.
Siguin, D., Ferreira, S., Froufe, L., Garcia, F., 1994. Smectites, the relationship between their properties and isomorphic substitution. J. Mater. Sci. 29, 4379–4384.
Tjong, S., 2006. Structural and mechanical properties of polymer nanocomposites. Mater. Sci. Eng. Res. 53, 73–197.

Ton-That, M.T., Ferrin-Sarazin, F., Cole, K.C., Bureau, M.N., Denault, J., 2004. Polyolefin nanocomposites: formulation and development. Polym. Eng. Sci. 44 (7), 1212–1219.

Torres Sánchez, R.M., Falasca, S., 1997. Specific surface and surface charges of some Argentinean soils. Z. Pflaz. Boden. 160, 223–226.

Vaia, R.A., Giannelis, E.P., 1997. Polymer melt intercalation in organically-modified layered silicates: model predictions and experiment. Macromolecules 30, 8000–8009.

Vazquez, A., Lopez, M., Kortaberria, G., Martin, L., Mondragon, I., 2008. Modification of montmorillonite with cationic surfactants. Thermal and chemical analysis including CEC determination. Appl. Clay Sci. 41, 24–36.

Xiong, J., Zheng, Z., Jiang, H., Ye, S., Wang, X., 2007. Reinforcement of polyurethane composites with an organically modified montmorillonite. Composites: Part A 38, 132–137.

Yamaguchi, M., Arakawa, K., 2006. Effect of thermal degradation on rheological properties for poly(3-hydroxybutyrate). Eur. Polymer J. 42, 1479–1486.

Zhang, X., Lin, G., Abou-Hussein, R., Hassan, M.K., Noda, I., Mark, J., 2007. Some novel layered-silicate nanocomposites based on a biodegradable hydroxybutyrate copolymer. Eur. Polymer J. 43, 3128–3134.

Zenggang, W., Chixing, Z., Na, Z., 2002. The nucleating effect of montmorillonite on crystallization of nylon 1212/montmorillonite nanocomposite. Polym. Test. 21, 479–483.